

## Tropical–Extratropical Interaction Associated with the 10–25-day Oscillation over the Western Pacific during the Northern Summer

Yoshiki FUKUTOMI<sup>1</sup> and Tetsuzo YASUNARI<sup>2</sup>

*Institute of Geoscience, University of Tsukuba, Tsukuba, Japan*

*(Manuscript received August 2000, in revised form 11 January 2002)*

### Abstract

Ten years (1986–1995) of ECMWF analyses and NOAA outgoing longwave radiation (OLR) data were used to investigate intraseasonal tropical–extratropical interactions on timescales of 10–25 days in the western Pacific region during Northern Hemisphere (NH) summer. Composite analyses were performed separately for the early summer (June–July) and mid-summer (August). The analyses were based on the OLR index in the base region (the South China Sea), and help describe the seasonal characteristics of circulation associated with tropical convection. Localized Eliassen–Palm (E–P) fluxes were used to diagnose eddy–mean flow interactions.

Composite circulation patterns associated with enhanced convection on a 10–25-day timescale for June–July were significantly different from those for August. June–July composites show a significant Rossby wave train in both the lower and upper troposphere, extending from the convective region into the North Pacific along the mean westerly flow. In the lower troposphere, subtropical circulation anomalies as part of this wavetrain propagate southwestward along the subtropical duct. Tropical–extratropical linkage is less pronounced during August. Circulation structures in August in both the lower and upper troposphere are different from those of June–July; Rossby waves do not emanate from the South China Sea and low-level subtropical circulation anomalies show no southwestward phase propagation.

Energy conversion between eddy and seasonal mean flow for each season was computed to investigate the role of the time-mean flow in maintaining the 10–25-day transient eddies. In the lower troposphere, barotropic processes dominate the conversion from the time-mean flow to eddies in the exit region of tropical monsoon westerlies for both June–July and August. In the subtropics, baroclinic processes sustain the eddies. Moist baroclinic processes associated with eddy horizontal latent heat transport are important in increasing the potential energy available to eddies, especially during June–July. In the upper troposphere, barotropic conversion of kinetic energy from eddies into the time-mean flow is most notable in the East Asian subtropics to the north of the South China Sea. This suggests that increased eddy activity due to tropical convection is an important source of energy for the mean flow.

### 1. Introduction

The characteristics of higher-frequency intraseasonal waves linked to tropical convection, and their associated tropical–extratropical interactions, have been the subject of considerable interest in the past decade. Intraseasonal oscillations on so-called submonthly (about 6–30-day) timescales (e.g., Meehl et al. 1996) are recognized as an important component of the subseasonal atmospheric variability as same as the Madden–Julian Oscillation (MJO: about

---

1 Present affiliation: Frontier Research System for Global Change, Institute for Global Change Research, JAMSTEC Yokohama Institute for Earth Sciences, Yokohama 236-0001, Japan.

2 Corresponding author: Tetsuzo Yasunari, Institute of Geoscience, University of Tsukuba, Tsukuba, 305-8571, Japan.  
E-mail: yasunari@atm.geo.tsukuba.ac.jp  
Additional affiliation: Frontier Research System for Global Change.

© 2002, Meteorological Society of Japan

30–60 days) (e.g., Madden and Julian 1972, 1994). Vincent et al. (1998) presented a comprehensive review of observational work on submonthly scale variability. After Kiladis and Weickmann (1992a, b) identified significant linkages between tropical deep convection and large-scale circulation, a series of studies clarified the nature of tropical convective disturbances and the associated tropical–extratropical interactions on submonthly timescales. For example, Kiladis and Weickmann (1992b), Kiladis (1998), and Matthews and Kiladis (1999a) investigated midlatitude Rossby-wave forcing of tropical convection over the eastern Pacific. Meehl et al. (1996) showed that this type of Rossby-wave propagation into the tropics could excite intertropical convergence zone (ITCZ) convection and generate equatorial Rossby waves (e.g., Kiladis and Wheeler 1995; Numaguti 1995; Wheeler and Kiladis 1999). Kiladis et al. (1994) and Meehl et al. (1996) showed that these equatorial Rossby waves propagate westward along the equator into the western Pacific, and contribute to tropical westerly wind bursts accompanied by flare-ups of deep convection. Kiladis and his collaborators used the regression composite method to elucidate the role of submonthly timescale waves during NH winter. In addition, Mo (1999, 2000) reported that midlatitude waves over the Pacific, which are responsible for North American precipitation variability on a similar timescale, link to westward-propagating convection in the tropical Pacific. In particular, Mo (2000) examined the teleconnection between the Pacific intraseasonal mode and North American rainfall during the NH summer. Relationships between extratropical circulations on submonthly timescales and tropical and subtropical convection in the South Pacific convergence zone (SPCZ) (e.g., Kiladis and Weickmann 1992b; Schrage and Vincent 1996; Vincent et al. 1997) and the South Atlantic convergence zone (SACZ) (e.g., Kiladis and Weickmann 1992a, 1997; Liebmann et al. 1999) have also been studied.

The relationship between tropical deep convection and extratropical Rossby waves at submonthly timescales is two-way. Tropical convection forces downstream extratropical waves, and the propagation of waves from midlatitudes toward the tropics induces tropical or subtropical convection. Tropical–extratropical interac-

tions on submonthly timescales and the roles of the interactions in tropical and subtropical variability during the NH summer over the Pacific basin have not been studied in depth. A summertime extreme of convective activity in this frequency range occurs over the western tropical Pacific region including the South China Sea (e.g., Chen and Chen 1995; Vincent et al. 1998; Kiladis 1998). Our study examines how this convection is triggered and the impact that it has on large-scale circulation. It seems reasonable to expect that a tropical–extratropical interaction similar to those mentioned above plays an important role in tropical and subtropical monsoon activities.

In an earlier study, Fukutomi and Yasunari (1999, hereafter FY99) suggested that a two-way tropical–extratropical interaction on a 10–25-day timescale exists over the western Pacific during the early summer (June–July). They examined the relationships between tropical convection over the South China Sea and large-scale circulation. They showed a lower- and upper-tropospheric wavetrain with zonal wavenumber 5~6 scale arcing into North Pacific midlatitudes and suggested that the wavetrain is amplified as a Rossby-wave response following enhanced (suppressed) convection over the South China Sea. A subtropical ridge (trough) that is part of this wavetrain modulates the subtropical cloud activities over the Baiu frontal zone (BFZ). In the lower troposphere, a subtropical anticyclonic (cyclonic) circulation anomaly propagates southwestward into the South China Sea region where the anomaly can suppress (enhance) subsequent convection. They proposed that this two-way interaction between tropics and extratropics is the dominant feature in the western Pacific during this season. Furthermore, seasonal (June–July) mean westerlies continuously extend from the tropical monsoon region to the North Pacific, acting as a duct that allows southwestward phase propagation of lower tropospheric waves from the subtropics to the tropics.

FY99, however, considered data only for four early summer seasons, from 1991 through 1994, and ignored the behavior of 10–25-day disturbances during the mid-summer (August). Most previous studies of summertime intraseasonal disturbances considered a standard season (JJA). As will be shown in later sections, how-

ever, the background basic state on which the intraseasonal disturbances are superimposed differs considerably between early and mid-summer over the western Pacific. The changes in the mean background flow that occur as the summer evolves may affect the development of tropical convective disturbance and their associated large-scale circulation over the western Pacific. Therefore, the structures of tropical 10–25-day disturbances and associated large-scale circulation and their differences should be investigated for each phase of the summer season to understand the character of subseasonal circulation systems in this region.

FY99 also speculated that dynamical interactions with the time-mean flow helped amplify and maintain 10–25-day waves. Few studies have assessed this interaction between sub-monthly scale eddies and the time-mean flow in the western Pacific during NH summer. Kawamura and Murakami (1995) examined the interaction between MJO-timescale eddies and the mean monsoon flow in the lower troposphere. They suggested that eddies are maintained mostly by barotropic instabilities in the tropics and by baroclinic instabilities in mid-latitudes. It is natural to question whether similar mechanisms exist to maintain 10–25-day eddies.

This study extends FY99. Space-time structures of convection and large-scale circulation anomalies at the 10–25-day time scale over the western Pacific are detailed to identify features in two seasons. Composite relationships between tropical convection and large-scale circulations on the 10–25-day timescale during early summer (June–July) and mid-summer (August) are used to isolate the dominant circulation patterns associated with tropical convection for early and mid-summer. Composites are constructed using data from 1986 through 1995. The structure and behavior of 10–25-day convective disturbances and associated waves in the subtropical and extratropical latitudes can be discerned. The target convection amplifies over the South China Sea. We will identify the seasonal dependence of the large-scale circulations associated with tropical convection over the South China Sea. Localized Eliassen–Palm (E–P) flux diagnostics (Trenberth 1986) and their application (Kawamura and Murakami 1995) are then used to assess eddy–mean flow

interactions and to quantify the role of the mean flow in maintaining 10–25-day eddies. Eddy forcing of the mean flow is also investigated.

This paper is organized as follows. Section 2 describes data sources and processing. In Section 3, characteristics of disturbances and of the mean flow in the two seasons (June–July and August) are given. In Sections 4 and 5, composite relationships between the 10–25-day convective events and large-scale circulation over a selected base region are presented. The structure and characteristics of disturbances are also outlined in these sections. Section 6 includes diagnostics of the eddy–mean flow interactions and an evaluation of the dynamical interaction between the eddy and time mean flow. The paper concludes with a summary and discussion in Section 7.

## 2. Data sources and processing

This study uses the same datasets as FY99. Meteorological data (zonal and meridional wind, temperature, geopotential height, and relative humidity) at ten standard pressure levels (1000, 850, 700, 500, 400, 300, 250, 200, 150, 100 hPa) were extracted from the European Center for Medium-Range Weather Forecasts (ECMWF)/World Climate Research Programme (WCRP)/Tropical Ocean-Global Atmosphere (TOGA) BASIC LEVEL III operational analyses from 1986 through 1995. We use uninitialized data defined on a  $2.5^\circ$  lat-long grid. The original temporal resolution was twice daily (0000 and 1200 UTC). Humidity data were only available up to 300 hPa. Further details on the ECMWF data are provided in Trenberth and Olson (1988). Specific humidity was computed from relative humidity and temperature. A daily mean that eliminated the diurnal cycle was computed using an average of the twice-daily data. Streamfunctions were computed from the horizontal winds using R25 truncation.

This study also uses outgoing longwave radiation (OLR) data as a proxy for convection. The interpolated OLR dataset for times overlapping the ECMWF data was obtained from the National Oceanic and Atmospheric Administration (NOAA)/Climate Diagnostics Center (CDC) and has global coverage on a  $2.5^\circ$  lat-long grid.

The first step in the data processing was to remove the seasonal trend from time series of all elements for the five-month period May to Sep-

tember. The seasonal trend was computed by the least squares method as a quadratic curve for the five months. A Butterworth band-pass filter (Kaylor 1977) with six poles was then applied to the time series of each perturbation quantity to filter temporally into the 10–25-day band. The 10–25-day band was chosen because FY99 and Fukutomi (2000) showed that this frequency was prominent. In addition, the 10-day low-pass cut off and 25-day high-pass cut off eliminate synoptic- and MJO-timescale fluctuations, respectively. The 10–25-day timescale is similar to those used by Kiladis (6–30-day) and by Vincent et al. (1998) (6–25-day).

### 3. Differences in transient disturbance activity between June–July and August

The 10–25-day disturbance activity is computed from the OLR variance and the perturbation kinetic energy (PKE). The PKE is derived from band-pass filtered meteorological data and is expressed as in Matthews and Kiladis (1999a), i.e.,

$$\text{PKE} = \frac{1}{2} \overline{(u'^2 + v'^2)}, \quad (3.1)$$

where  $u$  and  $v$  are the zonal and meridional wind components,  $\overline{(\cdot)}$  denotes the time mean, and  $(\cdot)'$  is the time deviation with 10–25-day band-pass filtering.

PKE and OLR variance distributions and background mean fields are displayed in Figures 1 and 2, respectively. From these figures, we can determine where transient disturbances are most common in June–July and August in the western Pacific. The PKE fields at 850 hPa (Fig. 1a) show a maximum oriented southwest–northeast from the South China Sea to the North Pacific during June–July. This maximum PKE band parallels the mean low-level westerlies (as seen in Fig. 1c). In the tropics, the maximum PKE is over the northern South China Sea. The OLR variance field for June–July (Fig. 1b) shows maximum convective activity on the 10–25-day timescale over the South China Sea and Bay of Bengal, in agreement with FY99. Past studies have shown that the peak OLR variance for the 10–25-day timescale occurs over these regions during the summer (JJA) (e.g., Kiladis and Weickmann 1997; Vincent et al. 1998). Here, mean fields for June–

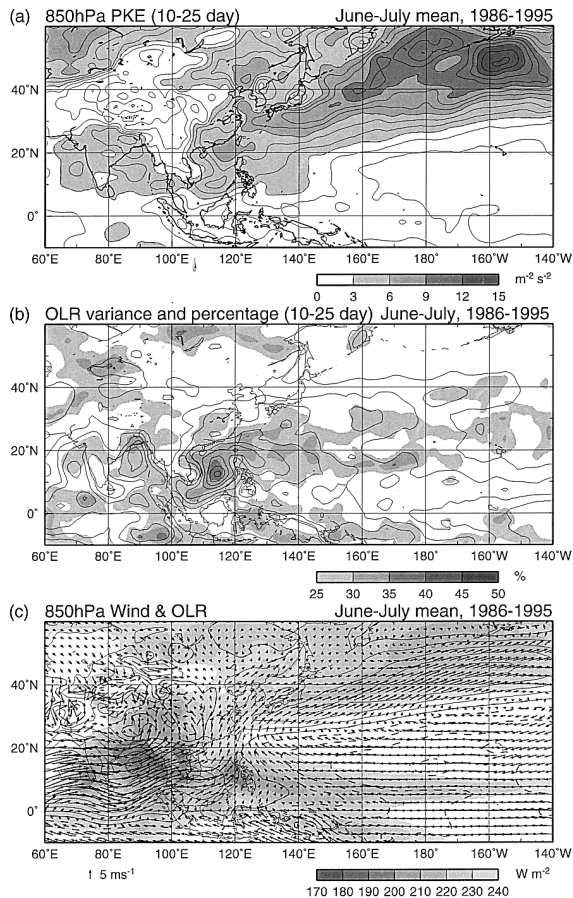


Fig. 1. Distributions of mean fields in June–July 1986–1995. (a) The 10–25-day perturbation kinetic energy (PKE) at 850 hPa. The contour interval is  $1 \text{ m}^2 \text{ s}^{-2}$ . Shading indicates PKE less than  $3 \text{ m}^2 \text{ s}^{-2}$ . (b) Variance and percentage variance of 10–25-day filtered OLR. The contour interval is  $100 \text{ W}^2 \text{ m}^{-4}$ . (c) Mean OLR and 850-hPa wind vectors and isotachs of zonal wind. Negative contours are dashed. The regions of OLR values less than  $240 \text{ W m}^{-2}$  are shaded.

July (Fig. 1c) are consistent with the mature phase of the south and southeast Asian monsoons and the Baiu front, which is marked by quasi-stationary subtropical cloud activity in East Asia. The monsoon westerlies and the tropical easterlies on average meet over the Philippines, where the highest disturbance activity in the tropics is found.

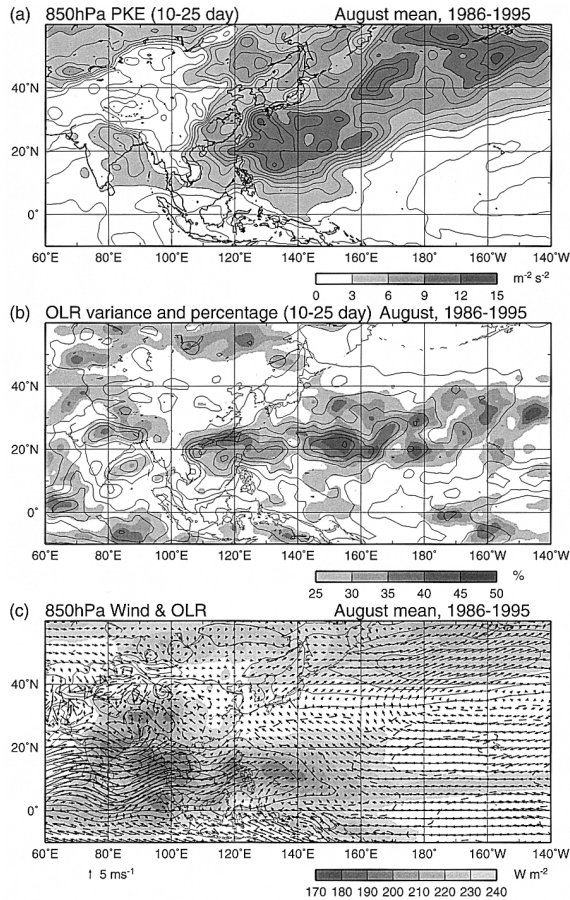


Fig. 2. As in Fig. 1, but for August 1986–1995.

A striking feature during August is the eastward extension of the PKE band from the South China Sea to the western Pacific in the tropics and subtropics (Fig. 2a). The tropical portion of this PKE maximum exists in conjunction with a large OLR variance (Fig. 2b) at  $130^{\circ}$ – $150^{\circ}$ E. Active regions of convection expand eastward from the South China Sea to the tropical western Pacific as the mean tropical monsoon westerlies penetrate into the tropical western Pacific near  $150^{\circ}$ E (Fig. 2c). This eastward shift from June–July through August is similar to the shift for MJO-scale eddies demonstrated by Kawamura and Murakami (1995).

In summary, enhanced disturbance activity in the lower troposphere on the 10–25-day timescale is concentrated in the exit region of monsoon westerlies, i.e., where the zonal gradient of the mean westerlies is negative. The

mean fields (Fig. 2c) change dramatically in August, as noted by many previous studies (e.g., Matsumoto 1992; Murakami and Matsumoto 1994). The distribution of the transient eddies also changes in association with this structural change in the mean flow. Disturbance activity in the tropics is closely related to the spatial distribution of the mean flow, as shown by Webster and Yang (1989).

#### 4. Composite structures during June–July

Compositing was used to determine the space–time structures of disturbances associated with tropical convection on 10–25-day timescales. The composite procedure used was nearly identical to that of FY99. The reference OLR time series in the base region  $10^{\circ}$ – $20^{\circ}$ N,  $110^{\circ}$ – $120^{\circ}$ E (the South China Sea) was adopted as a convective index. As noted in Section 3, this is the region of highest convective activity at the 10–25-day timescale as shown in the OLR variance (Figs. 1 and 2). Composite maps include eight states (Categories 1 through 8) that correspond to individual phases of the convection lifecycle over the base region. When the negative (positive) extreme of the OLR index averaged over the base region exceeded  $-1.0$  ( $1.0$ ) standard deviations, that extreme was assigned to Category 3 (Category 7). This procedure holds in all composites in this analysis. The mean time span between two subsequent phases is approximately 1.5–2 days. Composite fields were prepared for both June–July and August to reveal the structures and characteristics of disturbances during these times. The composite patterns are significant at the 95% confidence level as revealed by a standard  $t$ -test.

##### 4.1 Horizontal structures

Two-way interactions between tropics and extratropics over the western Pacific in June–July were outlined in Section 1. The interactions are present in the space–time structures of the 10–25-day wave disturbances and the related tropical–extratropical interactions during June–July as discussed in FY99. Composites in FY99, however, were based on a relatively small number of June–July cases during 1991–94. In the present analysis, we produce composite fields from a total of 32 cases over 10

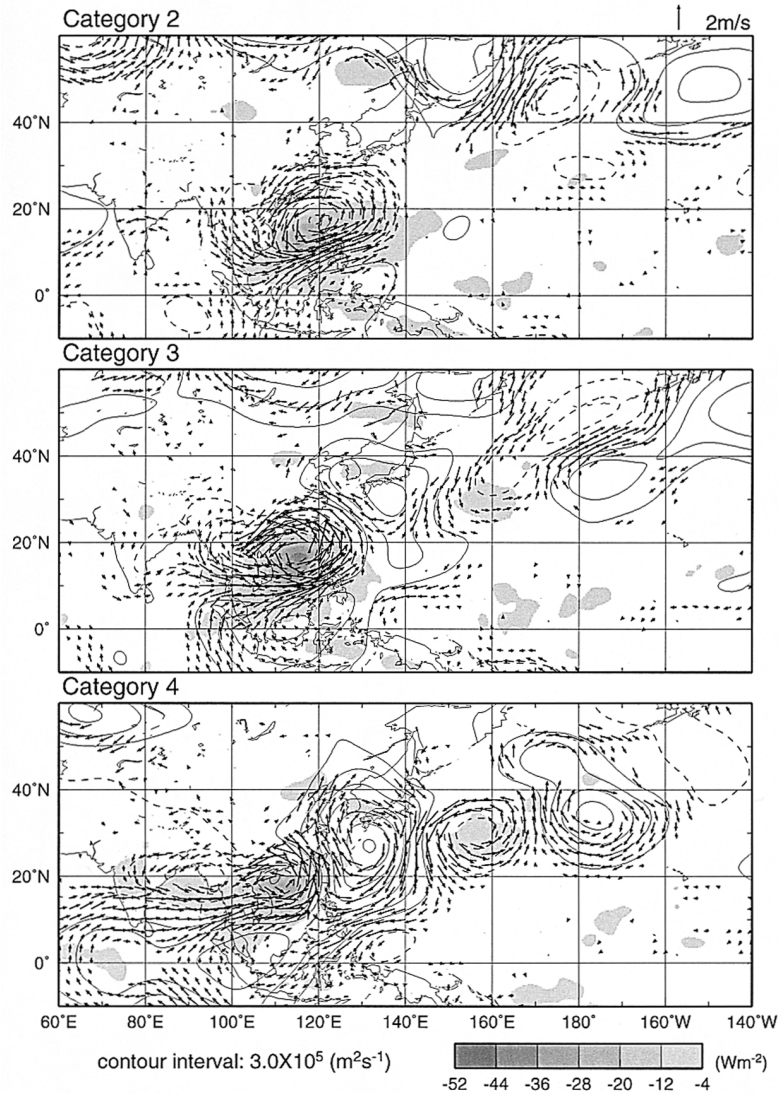


Fig. 3. The composite OLR, 850-hPa streamfunction and vector wind anomalies for Categories 2, 3, and 4 for June–July based on the OLR index in region  $10^{\circ}$ – $20^{\circ}$ N,  $110^{\circ}$ – $120^{\circ}$ E. The contour interval is  $3.0 \times 10^5 \text{ m}^2 \text{ s}^{-1}$ . OLR anomalies less than  $-4 \text{ W m}^{-2}$  are shaded. Only locally statistically significant wind vectors are shown.

years (1986–1995). June–July composites are based on the OLR index for the South China Sea because the OLR variance is largest in this region during June–July. The composites are comparable to those for August, as discussed in Section 5.

This section focuses only on phases during enhanced convection (Categories 2–4), as characteristics of the entire composite lifecycle (from Category 1 through 8) are described in detail by FY99. Figure 3 shows horizontal composites of

OLR, 850-hPa wind vector, and streamfunction anomalies for Categories 2, 3, and 4, bracketing the peak in convection over the base region. The relationship between the convection represented by negative OLR anomalies in the South China Sea and the large-scale circulation anomalies is present, as in FY99. Following the convective peak (Category 3), a wave-train clearly emanates from the convective region into the North Pacific. This wave structure shows good agreement with FY99, but the

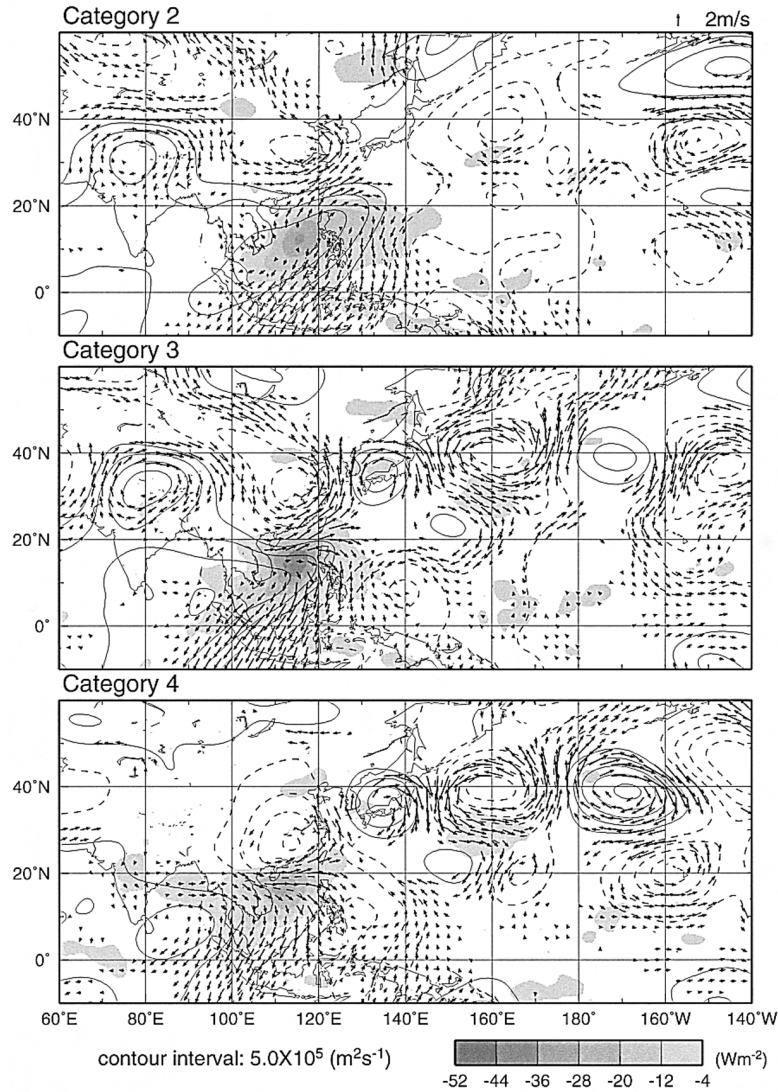


Fig. 4. As in Fig. 3, but for 200-hPa circulation fields. The contour interval is  $5.0 \times 10^5 \text{ m}^2 \text{ s}^{-1}$ .

anomalies described here are smoother than in FY99, reflecting the larger number of samples used to construct the composites. The cyclonic or anticyclonic circulation anomalies that are part of this wavetrain are amplified along the low-level mean westerlies that extend from the tropics to midlatitudes. Patterns of circulation and OLR anomalies for Categories 6, 7, and 8 (not shown) are reversed from Fig. 3. These two categories represent the phases during which convection is suppressed over the South China Sea. During the composite cycle (Category 1 through 8) provided by FY99, rotational wind anomalies propagate southwestward from the

subtropics to the tropics, and precede the subsequent suppression or enhancement of convection over the base region. These features are also clear in the present composite life cycle. We made composites based on the region  $10^\circ\text{--}20^\circ\text{N}$ ,  $130^\circ\text{--}140^\circ\text{E}$  (not shown); a downstream wave structure similar to that in Fig. 3 resulted.

Figure 4 is similar to Fig. 3, but shows the 200-hPa wind fields. The composite map shows a wavetrain developing away from the north of the convection center, crossing the midlatitude Pacific. These composite wave anomalies resemble those in FY99 and Mo (2000). The cross-equatorial outflow anomalies into the Southern

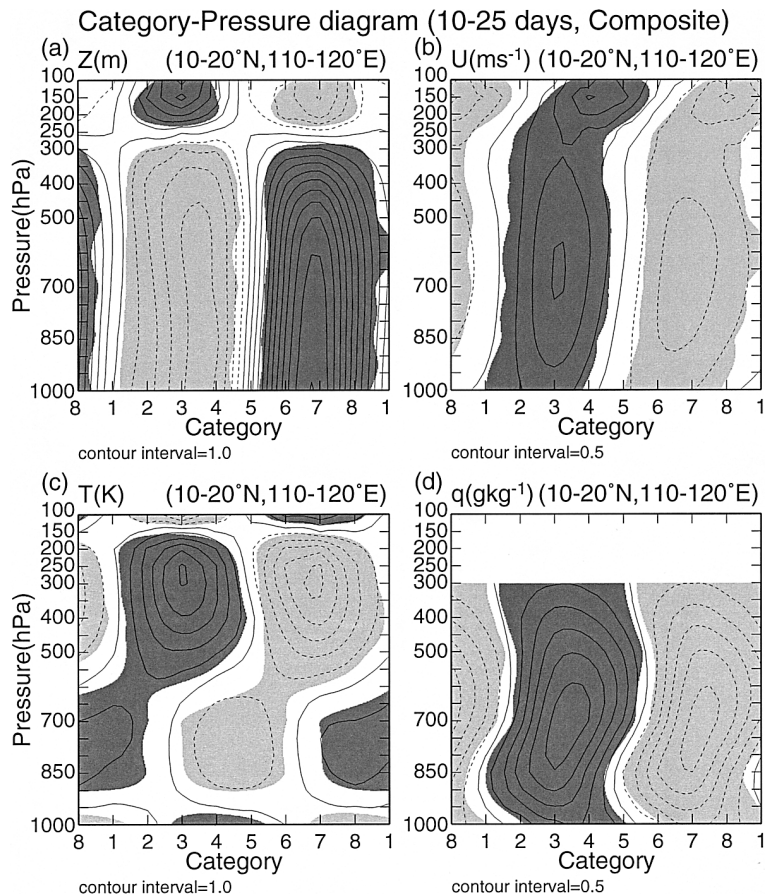


Fig. 5. Category–pressure diagrams in the region  $10^{\circ}$ – $20^{\circ}$ N,  $110^{\circ}$ – $120^{\circ}$ E of the composite values of the 10–25-day filtered (a) geopotential height (m), (b) zonal wind ( $\text{m s}^{-1}$ ), (c) temperature (K), and (d) specific humidity ( $\text{g kg}^{-1}$ ). Dark (light) shading represents positive (negative) significant values.

Hemisphere and the southwesterly outflow anomalies into midlatitudes are strongest over the convection in Categories 3 and 4. These outflows are the divergent response to the convection. Fukutomi (2000) produced composites of velocity potential and the divergent component of wind anomalies at 200 hPa. These composites show that the upper-level divergent outflow is displaced from the convection center, which confirms the presence of an immediate response to the convectively produced diabatic heating over the South China Sea in the form of an atmospheric circulation.

#### 4.2 Vertical structures

We examined the vertical structure of the 10–25-day disturbance using cross sections (category–pressure) of temperature, specific hu-

midity, geopotential height, and zonal wind perturbations averaged along  $10^{\circ}$ – $20^{\circ}$ N,  $110^{\circ}$ – $120^{\circ}$ E, at pressure levels from 1000 to 100 hPa in the vertical. The vertical section of geopotential height (Fig. 5a) shows an equivalent barotropic structure with negative anomalies extending to about 300 hPa around Category 3. This suggests that a deep cyclonic vortex in the low and middle troposphere dominates over the base region. A sign change occurs between 300 and 200 hPa, and positive anomalies (an anticyclone) are pronounced in the layers above 250 hPa. A similar pattern of anomalies, but of opposite sign, occurs around Category 7. The zonal wind anomalies (Fig. 5b) show deep westerlies with a maximum at 700 hPa at a position corresponding to the southern part of the low-level monsoon trough in Fig. 3. These deep

westerlies are similar to those accompanying wintertime submonthly-scale waves coupled with convection in the tropical central Pacific, as described by Kiladis et al. (1994) and Meehl et al. (1996). The upper-level easterlies that strengthen in the 200–100-hPa layer, capping the deep westerly flow, show the increase of the vertical easterly shear in the middle to upper troposphere.

The structures of composite variables over the base region have also been examined for Category 3 using longitude–pressure and latitude–pressure diagrams (Fukutomi 2000). The phase structures of the anomalous geopotential height and zonal winds in the zonal direction show little tilt in the vertical. Pronounced poleward phase tilts with height are observed in latitude–pressure diagrams in the 300–150-hPa layer. Phase nodes in the upper troposphere near the tropopause imply the predominance of first baroclinic modes associated with the strong convective disturbance. Although Lau and Lau (1990) showed a northwestward phase tilt with height over the western Pacific of the geopotential height and vorticity anomalies associated with synoptic-scale disturbances with period of less than 10 days, our composites do not have such a structure. This is one of the differences between 10–25-day intraseasonal disturbances and shorter-period disturbances.

Temperature anomalies (Fig. 5c) have a large maximum between 500 and 200 hPa, above the low-level cyclonic circulation associated with the peak convection (Category 3) in Figure 3. This upper-level warming is probably caused by condensation. Negative temperature anomalies in the lower troposphere under the peak in the upper-layer warming may arise from adiabatic cooling associated with ascent. A deep layer of moist air embedded in the low-level cyclonic circulation during the former half cycle appears in the specific humidity field (Fig. 5d). These moist conditions are probably organized by cyclonic and convergent inflow in the lower troposphere (see Fig. 3). An increase in moisture in the lowest (1000–850-hPa) layer slightly precedes the peak in convection. Temperature and specific humidity perturbations create upper warm- (cool-) and lower moist- (dry-) core structures within cyclonic (anticyclonic) regions during times of enhanced (suppressed) convection.

## 5. Composite structure during August

Composites are prepared for OLR and wind fields in August for comparison to those of June–July. August composites use the same base region as June–July composites do. This region occurs where the relative maxima of OLR variance (Fig. 2a) and PKE (Fig. 2b) are located. Figure 6a shows horizontal composites for Category 3 OLR and winds at 850 hPa using the South China Sea base region. Ten cases are averaged to produce this composite. The disturbance does have a structure similar to that of June–July. However, a wavetrain emanating from the convection downstream into midlatitudes, as shown in Fig. 3, is not clearly seen associated with this peak in convection. Furthermore, southwestward phase propagation of circulation anomalies from the subtropics into the base region does not dominate from Category 1 through 8 (not shown). In the upper troposphere (Fig. 6b), weak northerly outflow away from the base region appears, but the midlatitude trough/ridge signals are weaker than in June–July. Statistically significant circulations over the Pacific are confined to the tropics and subtropics near the convection. Effects on large-scale circulations are weaker than during June–July.

## 6. Dynamical interaction between transient eddies and the mean flow

This study will show that the time-mean flow over the western Pacific creates a favorable environment for generating and maintaining high-frequency intraseasonal wave activity. Particular emphasis is placed on processes causing interactions between eddy activities with timescales of 10–25 days and the background time-mean flow in June–July and August.

As shown above and in FY99, tropical convection centered over the South China Sea is likely an important cause of the amplification of subtropical and midlatitude waves on 10–25-day timescales. The tropical–extratropical wave structure in the composites is representative of structures during the early summer. Wave amplification can be triggered by Rossby wave energy dispersion from the localized and periodic heat sources in the region. Li and Nathan (1994, 1997) and Hsu (1996) show that radiation of wave energy into the extratropics by en-

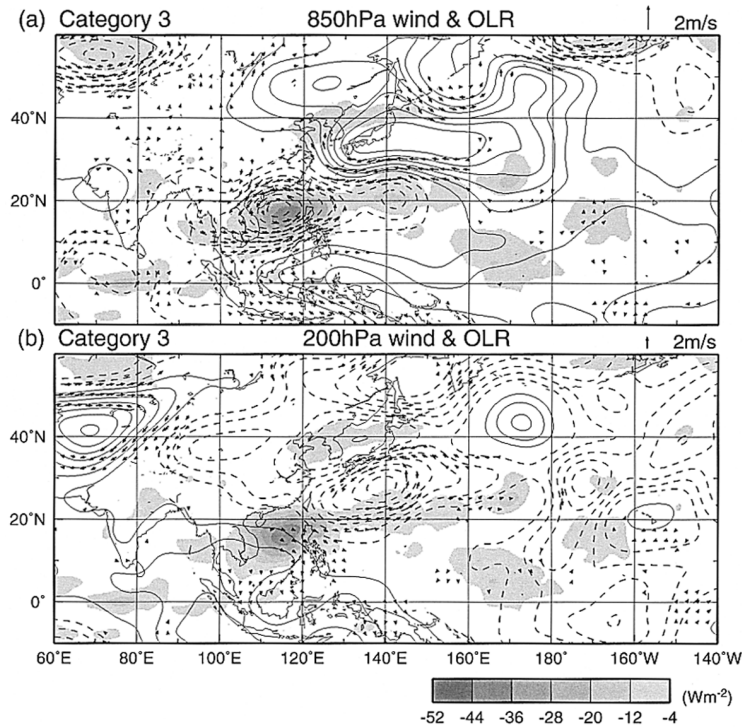


Fig. 6. (a) As in Fig. 3, but for Category 3 in August. (b) As in Fig. 4, but for Category 3 in August.

ergy advection and extraction of energy from the mean flow must both be considered when explaining the rapid growth and subsequent maintenance of tropically forced wave anomalies in the subtropics and midlatitudes. Li and Nathan used a spherical nondivergent barotropic model, and showed that the extratropical response to intraseasonal tropical forcing is affected by the background flow. If the extratropical response is manifest as disturbances on the locally unstable basic flow, the disturbances will amplify as they extract energy from the unstable base state. It is interesting that the disturbances in Li and Nathan have a timescale similar to those in this study, although their numerical experiment is for a different season.

Wave anomalies that are part of the downstream wave train retrograde (travel southwestward) from the subtropics equatorward to the tropics over the western Pacific, as shown in the low-level composite for June–July (Fig. 3). The anomalies then enhance or suppress convection over the South China Sea. These cyclonic or anticyclonic anomalies maintain their strength in the tropical and subtropical west-

erly duct region after the extreme in convective activity, as described by FY99. Maintenance of the 10–25-day waves could be linked to interactions between the mean flow and the 10–25-day transients within this westerly duct. This equatorward-propagating wave signature is one of the conditions necessary for exciting tropical convective disturbances.

The impact of the mean flow on the amplification of lower-tropospheric tropical disturbances over the South China Sea must also be considered. Kawamura and Murakami (1995) investigated the role of the deformed mean tropical and extratropical westerlies on eddy growth for MJO-scale tropical disturbances. They showed that stretching and shearing deformation in the exit region of the monsoon westerlies (in the tropics) supplies barotropic energy to the MJO-scale eddies. They further emphasized that baroclinic instability plays an important role in eddy maintenance in extratropical regions. In the next section, diagnostic tools based on dynamical theory are used to quantify the substantial contribution of the mean flow to the 10–25-day eddy activity. Tran-

sient eddy activity and its relationship to the mean flow in both the lower and upper troposphere for individual seasons are given.

### 6.1 *Transient wave activities: E–P flux diagnostics*

The net effect of the time-mean flow on transient eddies can be analyzed in terms of the Eliassen–Palm (E–P) flux, which was originally formulated by Hoskins et al. (1983) and subsequently modified by Hendon and Hartmann (1985), Plumb (1986), and Trenberth (1986, 1991). E–P flux vectors are a useful measure of intraseasonal or high-frequency (synoptic scale) transient eddies. The vectors describe the shape and propagation characteristics of eddies and their feedback onto the mean flow (Matthews and Kiladis 1999a). Recently, Kiladis (1998) and Matthews and Kiladis (1999a) used Hoskins’s  $\mathbf{E}_u$  vector to investigate submonthly scale (6–30-day) wave activities and tropical–extratropical interactions over the Pacific in NH winter. They showed extratropical forcing into the tropics over the eastern Pacific.

Hurrell and Vincent (1991) and Magaña and Yanai (1991) use  $\mathbf{E}_u$  represented by Trenberth (1991) to examine the eddy–mean flow interaction. This formulation is defined by transformed equations derived from the primitive momentum, thermodynamic, and continuity equations. Hurrell and Vincent (1991) used the three-dimensional vectors to investigate the impact of upper-level subtropical westerly maxima on transient eddies over the South Pacific. Magaña and Yanai (1991) used two-dimensional vectors to examine the tropical–midlatitude interaction on 30–60-day (MJO) time scales in the upper-troposphere around the mid-Pacific trough. Kawamura and Murakami (1995) extended Trenberth’s version and derived a modified  $\mathbf{E}_u$  for which the vertical (baroclinic) component includes a horizontal eddy latent heat flux effect. They used this modified E–P flux to assess the net effects of eddy moisture transport and organized latent heat release by eddies, and showed that the MJO-scale eddies are maintained through interactions with the low-level summer monsoon. Sobel and Bretherton (1999) applied the barotropic component of wave activity flux (Plumb 1986) to an investigation of synoptic-scale Rossby waves in the low-level flow over the western Pacific. The radiative part of

the Plumb flux is the same as that developed by Trenberth (1986), except for a pressure weighting. E–P flux diagnostics are a convenient way to examine eddy–mean flow interactions.

In this analysis, we use the two-dimensional  $\mathbf{E}$  vector as in Trenberth (1991). In spherical geometry,

$$\mathbf{E}_u = \left[ \frac{1}{2}(\overline{v'^2} - \overline{u'^2}), -\overline{u'v'} \right] \cos \phi, \quad (6.1)$$

where  $\phi$  denotes latitude. The horizontal (barotropic) components of  $\mathbf{E}_u$  consist of eddy momentum flux, and the horizontal vectors are parallel to the eddy group velocity relative to the mean flow (Trenberth 1986; Magaña and Yanai 1991). Horizontal vectors point in the direction of eddy energy propagation relative to the background flow. The vertical (baroclinic) components of  $\mathbf{E}_u$  include the meridional eddy sensible heat flux and vertical momentum flux (not shown).

The stationary Rossby wavenumber  $K_s$  is used diagnostically to represent the mean background state on which transients are superimposed. Following Hoskins and Ambrizzi (1993), this wavenumber is derived from the nondivergent perturbation vorticity equation for time-mean flow and is defined as

$$K_s = \left( \frac{\beta - \overline{U}_{yy}}{\overline{U}} \right)^{1/2}, \quad (6.2)$$

where  $\overline{U}$  is the temporal mean of the zonal wind,  $\beta - \overline{U}_{yy}$  is the temporal mean of the meridional absolute vorticity gradient, and  $K_s$  is the wavenumber at which a barotropic Rossby wave is stationary at a particular location in a given background zonal flow. The wavenumber acts as a refractive index for stationary Rossby waves (Kiladis 1998; Matthews and Kiladis 1999a). Originally,  $K_s$  predicted the location of waveguides for stationary Rossby waves (e.g., Karoly and Hoskins 1982; Hoskins and Ambrizzi 1993). However, Ambrizzi et al. (1995), Kiladis (1998), Matthews and Kiladis (1999a) show how  $K_s$  can qualitatively describe the effects of the base state on the propagation of high-frequency transient waves in the upper troposphere. In this study,  $K_s$  is also used to detect westerly ducts that act as waveguides for 10–25-day waves in both the lower and upper troposphere. Note that  $K_s$  is a complex

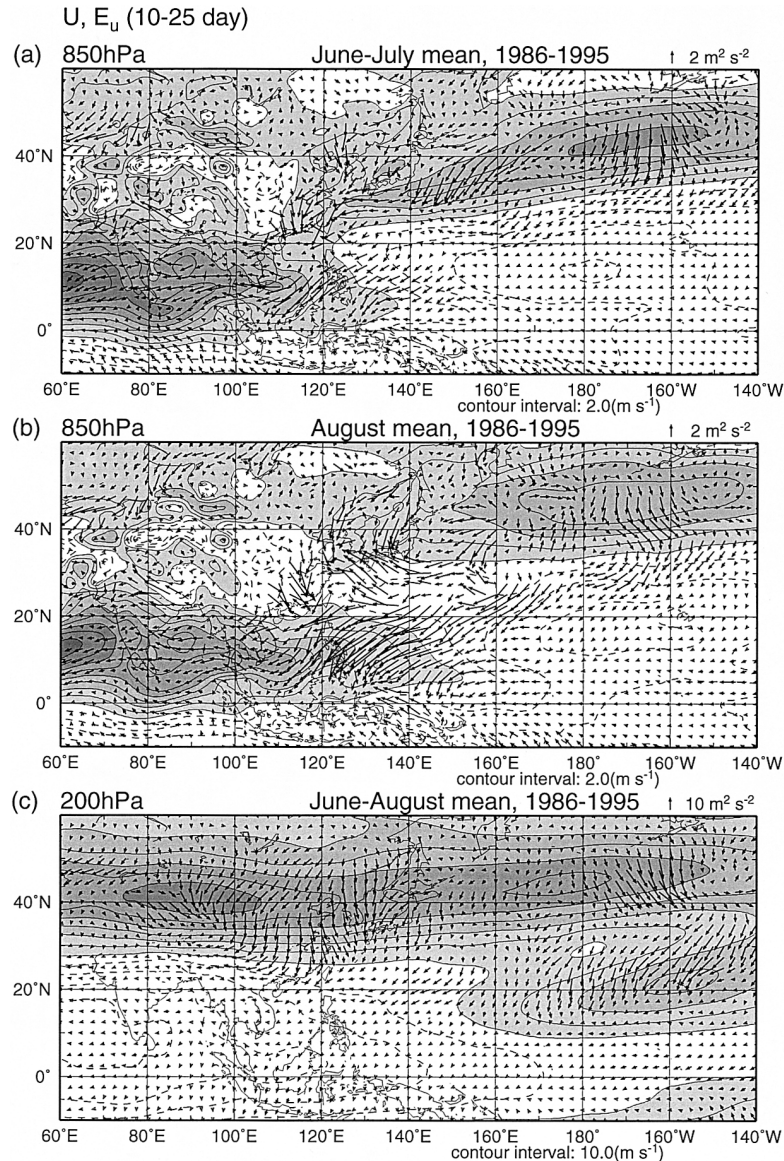


Fig. 7. Mean spatial distribution of  $E_u$  ( $\text{m}^2 \text{ s}^{-2}$ ) and zonal wind at (a) 850 hPa during June–July, (b) 850 hPa during August, and (c) 200 hPa during June–August. The contour interval is (a), (b)  $2 \text{ m s}^{-1}$ , and (c)  $5 \text{ m s}^{-1}$ . Regions of westerlies are shaded.

value; Rossby waves are evanescent in the imaginary  $K_s$  region.

Figure 7 shows the 10–25-day horizontal  $E_u$  vectors and the mean zonal winds at 850 hPa in June–July (Fig. 7a), August (Fig. 7b) and at 200 hPa in June–August (Fig. 7c) for 1986–1995 data over Asia and the Pacific. At 850-hPa in June–July (Fig. 7a),  $E_u$  vectors point westward and southwestward along the subtropical

and midlatitude westerlies over the western Pacific. In addition, increased southward fluxes are present at the low-level jet core over the central Pacific ( $30^\circ$ – $50^\circ\text{N}$ ,  $170^\circ\text{E}$ – $170^\circ\text{W}$ ).  $E_u$  vectors point southwestward in the westerly exit region of the tropical monsoon westerlies, and point westward to the east of Southeast Asia. These vectors suggest westward and southwestward eddy energy propagation rela-

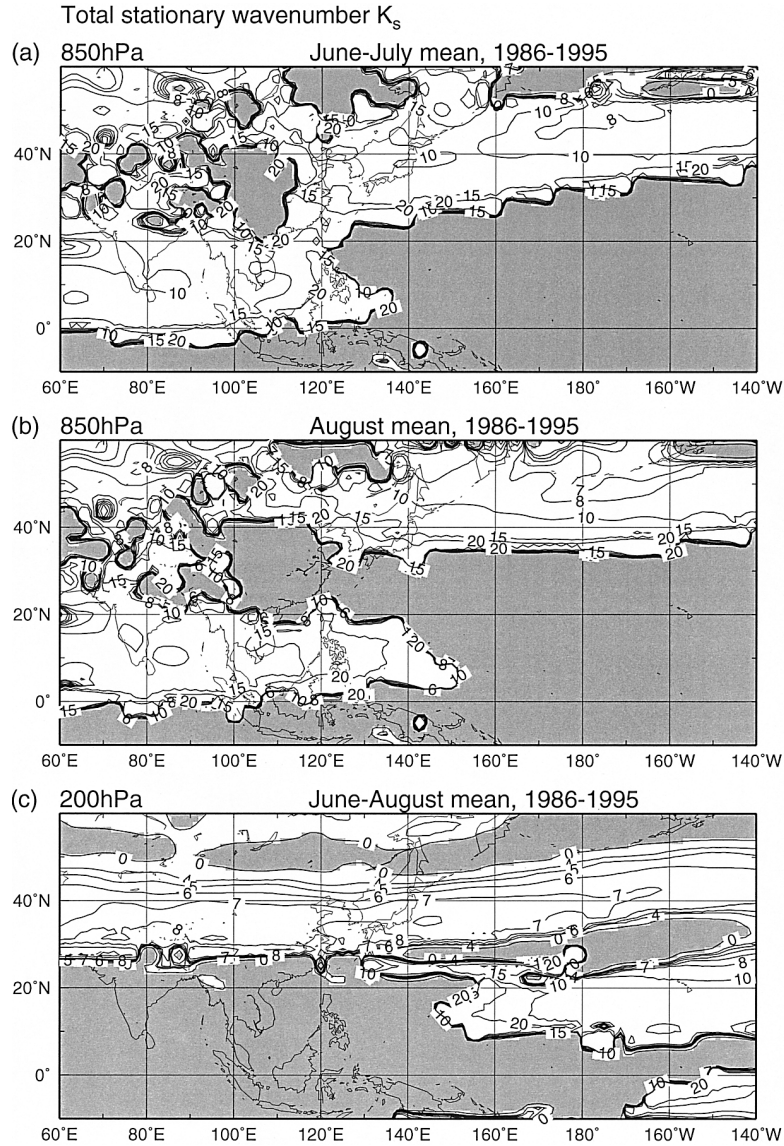


Fig. 8. Mean spatial distribution of  $K_s$  at (a) 850 hPa during June–July, (b) 850 hPa during August, and (c) 200 hPa during June–August. Contours are drawn at zonal wavenumbers 0, 4, 5, 6, 7, 8, 10, 15, 20. Regions of imaginary  $K_s$  are shaded.

tive to the mean flow, which is consistent with eastward and northeastward transient momentum transport within the tropical and subtropical westerly duct. These stronger components of  $\mathbf{E}_u$ , which are directed up the gradient of the mean westerly flow, may be associated with the seasonal ensemble disturbance amplification shown in Fig. 3. These flux vectors highlight the predominance of barotropic eddy–mean flow interactions in this area. Divergence of  $\mathbf{E}_u$  vec-

tors can be interpreted as a forcing on the westerly mean flow (Trenberth 1986). Such divergence occurs locally over the South China Sea and western Pacific north of 10°N. Convergence of  $\mathbf{E}_u$  implies mean easterly acceleration and occurs over southern China, near the Equator over the South China Sea and western Pacific (south of 10°N), and in the subtropics southeast of Japan. Figure 8a shows the distribution of  $K_s$  at 850 hPa in the same season. Regions of real

$K_s$  values are superimposed over climatological values for June–July tropical monsoon westerlies in South and Southeast Asia, and subtropical and midlatitude westerlies over the Pacific. The westerlies are a preferred region for Rossby wave energy propagation. Low-level composite wave anomalies (Fig. 3) are located along the distribution of real  $K_s$  values.

The distributions of  $\mathbf{E}_u$  and the mean zonal wind change significantly in the lower troposphere in August (Fig. 7b). One big change from the mean state of June–July is the eastward penetration of tropical monsoon westerlies into the western tropical Pacific near  $150^\circ\text{E}$ . Another change is the disappearance of a continuous duct (present in June–July) as the mean westerly component over the subtropics to the south of the East China Sea and Japan weakens. The  $\mathbf{E}_u$  vectors are characterized by a westward component directed upstream within the mean monsoon westerlies to the west of the South China Sea. The vectors have the same magnitude as in June–July. Near the exit region of this westerly current over the western tropical Pacific, where higher amplitude PKE is found (Fig. 2b), the southwestward pointing  $\mathbf{E}_u$  vectors are of larger magnitude than in June–July. Large westward and northwestward vectors are observed in the subtropics near Japan, where weak mean easterlies dominate. This region of subtropical easterlies corresponds to a region of imaginary  $K_s$  (Fig. 8b).

A waveguide at 200-hPa accompanying the westerlies and the real  $K_s$  values is present from June through August (Fig. 7c and Fig. 8c). A second duct exists over the tropical central and eastern Pacific. A region of imaginary  $K_s$  to the north of the midlatitude waveguide is a result of the negative meridional gradient of mean absolute vorticity. The  $\mathbf{E}_u$  vectors point southward, which indicates northward transport of zonal momentum due to eddies in the midlatitude waveguide. The largest vectors are near the core of the mean westerly flow over China and the East Asian coast ( $20^\circ$ – $50^\circ\text{N}$ ,  $100^\circ$ – $140^\circ\text{E}$ ). These southward and southwestward vectors converge over the East China Sea and north of the South China Sea. Eddy energy propagates southwestward from subtropics to tropics in the central Pacific westerly duct ( $10^\circ$ – $25^\circ\text{N}$ ,  $160^\circ\text{E}$ – $140^\circ\text{W}$ ). This energy propa-

gation may amplify the mid-Pacific trough as discussed by Magaña and Yanai (1991). Another feature to note is the group of southward and southeastward vectors in the exit region of the westerly jet ( $35^\circ$ – $50^\circ\text{N}$ ,  $180^\circ\text{E}$ – $150^\circ\text{W}$ ). Enhanced signals in  $\mathbf{E}_u$  vectors are indicative of the eddy–mean flow interaction at these locations. A separate examination of the upper-level distribution of  $K_s$  and  $\mathbf{E}_u$  for June–July and for August similar to that done for Fig. 8 (not shown) reveals little change in the structure of the upper-level waveguide from June through August.

## 6.2 Interaction between transients and the mean flow

The barotropic  $\mathbf{E}_u$  vector signatures associated with 10–25-day eddies along the lower- and upper-level waveguide implies transient–mean interactions in the westerly flow. A simple energetics analysis is performed to describe maintenance processes for the 10–25-day transient wave activities forced by eddy–mean interactions in barotropically and baroclinically unstable background flows. The formulation is obtained from the correlation between the three-dimensional localized E–P flux components and the horizontal and vertical shears of the mean zonal and meridional flows (Kawamura and Murakami 1995). It includes both barotropic and baroclinic eddy–mean interactions. An advantage of the formulation is that the effects associated with eddy moisture transport and the release of latent heat by eddies are included (see e.g., Salustri and Stone 1983). Following Kawamura and Murakami (1995), the local barotropic interaction is given by

$$\text{CK} = \left\{ -\frac{1}{2}(\overline{v'^2} - \overline{u'^2}) \frac{\partial \bar{u}}{\partial x} + \overline{u'v'} \frac{\partial \bar{u} \cos \phi}{\cos \phi \partial y} + \overline{u'v'} \frac{\partial \bar{v}}{\partial x} + \frac{1}{2}(\overline{v'^2} - \overline{u'^2}) \frac{\partial \bar{v} \cos \phi}{\cos \phi \partial y} \right\} \cos \phi. \quad (6.3)$$

Here  $\partial x = a \cos \phi \partial \lambda$ ,  $\partial y = a \partial \phi$ ,  $a$  is radius of the earth, and  $\lambda$  refers to longitude. Negative values of CK occur when kinetic energy is converted from the mean flow into eddies associated with the eddy momentum transport within the horizontal shear of the time-mean flow. The first (fourth) term of CK is the interaction between anisotropic eddies and zonal

(meridional) shear of the mean westerly (north-erly) flow. For example, if zonally elongated eddies ( $u'^2 > v'^2$ ) are embedded in a region where  $\partial\bar{u}/\partial x < 0$ , the first term becomes negative, which implies a conversion of perturbation kinetic energy from the mean. The second and third terms are typical forms of barotropic instability. If the eddy momentum transport ( $\overline{u'v'}$ ) is positive in the region of  $\partial\bar{v}/\partial x < 0$  and  $\partial\bar{u}/\partial y < 0$ , eddies can gain kinetic energy from the mean flow. In this analysis, barotropic interactions between the 10–25-day eddies and the time mean flow at both the 850-hPa and 200-hPa levels are estimated.

The eddy–mean interactions due to dry and moist baroclinic processes are calculated to examine the role of local baroclinic processes in maintaining eddies associated with the low-level 10–25-day waves. These interactions are defined as

$$\text{CAS} = \frac{f}{\sigma} \left\{ \overline{v'T'} \frac{\partial\bar{u}}{\partial p} - \overline{u'T'} \frac{\partial\bar{v}}{\partial p} \right\} \cos \phi, \quad (6.4)$$

$$\text{CAL} = \frac{L}{c_p} \frac{f}{\sigma} \left\{ \overline{v'q'} \frac{\partial\bar{u}}{\partial p} - \overline{u'q'} \frac{\partial\bar{v}}{\partial p} \right\} \cos \phi. \quad (6.5)$$

Where  $f$  is the Coriolis parameter,  $p$  is the pressure,  $T$  is the air temperature,  $q$  is the specific humidity,  $L$  is the latent heat of condensation, and  $c_p$  is the heat capacity at a constant pressure. The static stability parameter ( $\sigma$ ) is calculated using  $\sigma = RT/c_p p - (\partial T/\partial p)$ , where  $R$  is the gas constant. These are scalar products between the horizontal eddy sensible and latent heat fluxes (the horizontal part of three-dimensional  $\mathbf{E}$  vectors) and the vertical shear of the mean flow.

Negative CAS and CAL represent local baroclinic conversions from the mean available potential energy to eddy available potential energy and are proportional to the amount of horizontal sensible or latent heat transport and the vertical shear of the mean flows. The scalar product CAS is similar to the form used by Cai and Mak (1990) and Robinson (1993). The effect of latent heating induced by transient eddies can be isolated in the CAL estimation. In the subtropical and midlatitude lower tropospheres, northward eddy sensible heat and moisture fluxes ( $\overline{v'T'} > 0, \overline{v'q'} > 0$ ) can exist in regions of westerly vertical shear ( $\partial\bar{u}/\partial p < 0$ ), which is consistent with dry and moist baroclinic insta-

bility. Calculation of these values for the layer between 850 and 700-hPa levels follows methods in Kawamura and Murakami (1995).

Figure 9 shows CK at 850 and 200 hPa. At 850 hPa in June–July (Fig. 9a), large negative values (shaded region) extend from the South China Sea to the tropical western Pacific, the exit region of the tropical monsoon westerlies. There is a local minimum over southern China. This suggests that barotropic interaction with the mean flow is important in the growth and maintenance of 10–25-day waves in these regions. Estimation of each CK term indicates that the first term is of primary importance in this interaction (not shown). Cyclonic or anticyclonic circulations are zonally elongated in this tropical jet exit region (Fig. 3); this distribution allows mean to eddy energy conversions by the first term in CK. MJO-scale eddies are maintained in the same way in the same region, as discussed by Kawamura and Murakami (1995). In the subtropics near Japan, however, a band of positive CK values is located along the low-level mean subtropical westerly flow. An energy transfer from eddy to mean flow occurs at this low-level subtropical jet entrance.

In August (Fig. 9b), the barotropic energy conversion from the mean flow to the 10–25-day eddy increases over the western tropical Pacific from 130°–160°E, but decreases slightly over the South China Sea. As identified in the distributions of PKE and  $\mathbf{E}_u$ , the center of dynamical interaction between the mean flow and transient eddies in the tropics shifts from the South China Sea into the western Pacific. A weak mean to eddy energy transfer appears in the subtropics southwest of Japan.

At 200-hPa (Fig. 9c), large positive CK values persist throughout JJA over East Asia and the subtropical western Pacific. This maximum coincides with a large area of southward pointing  $\mathbf{E}_u$  vectors (Fig. 7c) located to the north of the region of convection (as in Fig. 3). This agrees with eddies supplying kinetic energy to the upper-level mean flow in the region. The second term in the CK equation is dominant south of the mean westerly core. Conversely, negative values lie north of the upper-level jet that extends from central Asia to eastern Pacific during JJA. The 10–25-day eddies receive kinetic energy from the mean within this region of negative CK values.

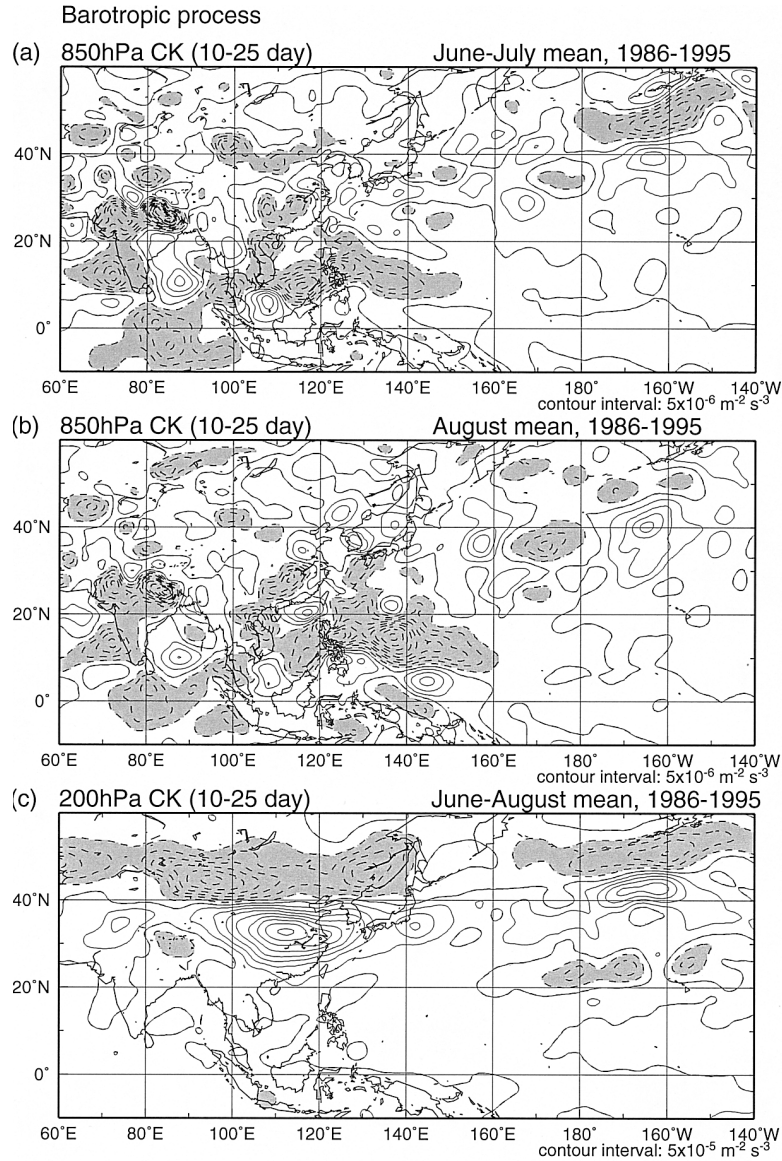


Fig. 9. Mean spatial distribution of barotropic eddy-mean flow interactions (CK) at (a) 850 hPa during June–July, (b) 850 hPa during August, and (c) 200 hPa during June–August. The contour interval is (a), (b)  $5.0 \times 10^{-6} \text{ m}^2 \text{ s}^{-3}$ , and (c)  $5.0 \times 10^{-5} \text{ m}^2 \text{ s}^{-3}$ . Negative values are shaded.

Baroclinic energy processes for June–July are shown in Figure 10. These processes dominate in the maintenance of 10–25-day perturbations in extratropical regions just as for the case of MJO-scale perturbations (Kawamura and Murakami 1995). The dry baroclinic process (CAS) (Fig. 10a) shows large negative values over the midlatitude North Pacific and eastern Asia, with comparatively smaller negative values over the subtropics near the East

Asian coast. Energy conversion from the mean available potential energy to the 10–25-day eddy available potential energy is associated with transient sensible heat fluxes in these regions. However, the small negative values of CAS over the subtropical western Pacific suggest that CAS is not important in maintaining 10–25-day waves in this region. In addition, a band of negative CAS values lies to the north of the composite wavetrain (Fig. 3). Significant

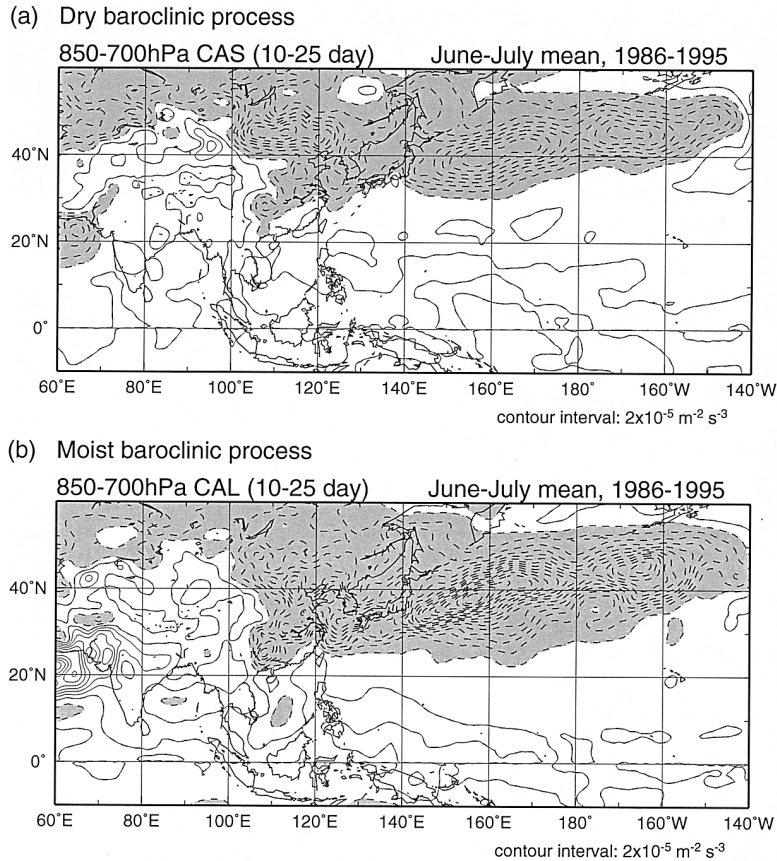


Fig. 10. Mean spatial distribution of (a) dry baroclinic (CAS) and (b) moist baroclinic (CAL) eddy-mean flow interactions. Contour intervals are  $2.0 \times 10^{-5} \text{ m}^2 \text{ s}^{-3}$ . Negative values are shaded.

values of CAS are not observed in the tropics, suggesting that CAS is unimportant for 10–25-day waves in the tropical lower troposphere.

The field of moist baroclinic processes (CAL) for June–July (Fig. 10b) is characterized by a zonally large area of negative values in the extratropical regions of Asia and the Pacific. The CAL contribution exceeds that of CAS in the subtropics and midlatitudes over the entire Pacific. The band of negative values is more pronounced over the North Pacific, and the areal extent of negative values of CAL is greater than that of CAS. This suggests that moist baroclinic processes are more important than dry baroclinic processes in maintaining 10–25-day eddies in the subtropics and midlatitudes during June–July. The prominence of baroclinic processes in the subtropics and midlatitudes is associated with the northward eddy sensible and latent heat transport within the mean

westerly vertical wind shear in the lower troposphere. This physical process is the same as for extratropical 40-day eddies (Kawamura and Murakami 1995). There is a region of negative CAL over the South China Sea, indicating that moist baroclinic eddy-mean flow interactions occurs locally within this very narrowly defined region.

The August distribution of baroclinically-forced eddy-mean flow interactions shows slight differences to that of June–July. The band of negative CAS values along the midlatitude westerlies shifts slightly to higher latitudes. This poleward shift is also observed in the negative CAL to the east of Japan. These shifts might be caused by a decrease in westerly vertical shear of the mean zonal wind in the subtropics and lower-midlatitudes, which is attributed to the northward shift of mean westerlies and the disappearance of a mean westerly com-

ponent in the subtropics. A negative CAL region overspreads the subtropical Pacific east of 140°E.

## 7. Summary and discussion

The structure and maintenance of 10–25-day disturbances over the western Pacific during summer were investigated. The disturbances were examined for two different seasons, namely June–July and August. The characteristics and behavior of anomalies in composites are identified for individual seasons and compared between seasons. E–P flux diagnostics and an energetics analysis reveal the roles of barotropic and baroclinic interactions between eddy and time-mean flow in maintaining transient wave activities in the lower troposphere. In particular, the forcing of transient eddies on the time-mean flow in the upper troposphere is also described.

Composites for June–July suggest significant relationships between tropical convection and extratropical circulations with timescales of 10–25 days. FY99 and this paper both suggest that tropical convection over the South China Sea can force subtropical and midlatitude circulations through a downstream Rossby wave response. Subsequent to the maximum enhancement (suppression) of convection, a downstream wave train is well developed toward the North Pacific along the subtropical and midlatitude westerlies in both the lower and upper troposphere. In the lower troposphere, a subtropical trough (ridge) is strengthened as part of this wavetrain. Subtropical anomalies in this wavetrain then move southwestward into the tropics, and initiate subsequent suppression (enhancement) of convection in the South China Sea region (cf., FY99). This two-way interaction between the tropics and the extratropics is a dominant feature of the convectively coupled 10–25-day waves during June–July.

August composites show the large-scale structure and behavior of circulation anomalies in the lower-troposphere to be considerably different from June–July. The downstream wavetrain emanating from the South China Sea is poorly defined in the August composites. Moreover, there is no evidence of southwestward anomaly propagation around this base region. The composite circulation anomalies have westward and northwestward tracking character-

istics. A two-way interaction mechanism does not become established in the lower troposphere during August.

The difference in the structure of the mean background flow between seasons may be responsible for the differences in the composite structures in the lower troposphere between June–July and August. During June–July, continuous mean westerlies extend from the tropics to midlatitudes in the lower troposphere. FY99 and this study suggest that this region of westerlies is a waveguide for the Rossby wavetrain and its southwestward phase propagation from the subtropics into the tropics over the western Pacific. During August, however, the structure of the low-level mean flow changes and the subtropical portion of the duct vanishes. This inhibits subtropical to tropical phase propagation. In addition, the absence of the arc-like downstream wavetrain may be related to the large-scale basic state, which includes a discontinuous waveguide between tropics and extratropics. The sensitivity of the extratropical response to transient convection acting on a basic state, and the phase propagation of forced waves can be checked using GCMs, as done by Jin and Hoskins (1995), Newman and Sardeshmukh (1998), and Matthews and Kiladis (1999b).

Eddy–mean flow interactions that maintain the 10–25-day waves are investigated. In the lower troposphere, barotropic processes maintain the 10–25-day eddies in the exit region of the monsoon westerly flow in the tropical western Pacific. Convectively coupled rotational disturbances are amplified in this region, not only by diabatic effects such as external heating (or cooling) associated with convection, but also by barotropic eddy–mean flow interactions. In contrast, the 10–25-day eddies supply kinetic energy to the mean flow over the subtropical western Pacific in June–July. Dry and moist baroclinic processes maintain the 10–25-day eddies in the subtropics and midlatitudes. The main contributor to the growth of the southwestward propagating waves during June–July is condensational heating produced by eddies embedded within a westerly vertical shear, especially in the subtropics. This subtropical duct with westerly vertical shear can support favorable conditions for wave maintenance. Baroclinic growth of the 10–25-day eddies

decreases over the subtropics south of Japan during August reflecting the weaker vertical shear in that season.

An energetics analysis shows that baroclinic processes associated with eddy sensible and latent heat transport are minor contributors to the maintenance or amplification of the low-level 10–25-day waves in the tropical domain. Barotropic processes dominate eddy–mean flow interactions in the tropical lower troposphere. Our results emphasize that barotropic processes and diabatic processes forced by convection are important in amplifying low-level waves in this region. A complete three-dimensional energetics analysis using composite anomalies and their life cycles, as done by Lau and Lau (1992), could clarify the relative roles of barotropic and baroclinic processes.

E–P flux diagnostics and energetics for the lower troposphere suggest that eddy energy accumulates in the exit region of tropical monsoon westerlies. This energy accumulation may be related to phase propagation of wave anomalies from other regions, as shown in the composites, and the energy can be enhanced through barotropic interactions with the mean flow. Negative longitudinal stretching shear of the zonal wind ( $\partial\bar{u}/\partial x < 0$ ) is effective for barotropic energy conversions from the mean flow to eddies in the exit region of the westerly monsoon. In particular, as a Rossby response to the convective heating, a wavetrain emanates from this energy-accumulation region into the extratropics during June–July. Webster and Chang (1988) proposed a similar energy accumulation–emanation mechanism.

Eddy–mean flow interactions in the upper troposphere have been analyzed. The 10–25-day eddies act as an energy source for the mean flow in the subtropics north of the tropical convection from 100°E to 150°E in the summer. There are large southward pointing  $\mathbf{E}_u$  vectors and barotropic conversion from eddy to mean kinetic energy over the subtropics in this longitudinal sector, and its location roughly corresponds to that of the amplified waves in the composites (Fig. 4). Enhanced eddies centered over the South China Sea produced by convection at this timescale may be an important energy source for the upper-level subtropical mean flow, especially in June–July.

We have focused on the structure and main-

tenance of the 10–25-day disturbances over the western Pacific domain in Northern Hemisphere summer, leaving other subjects to be examined later. As discussed by Hartmann et al. (1992), Schnadt et al. (1998), Heta (1990), and Chen and Weng (1999), the relationship between the occurrence of tropical cyclones and this higher-frequency intraseasonal oscillation in the tropics is an important subject for future research. Furthermore, the interaction between high frequency eddies and the MJO will be demonstrated in the future, as was done with the Northern Hemisphere winter case by Matthews and Kiladis (1999a). Scale interactions associated with the low-frequency waves, as demonstrated by Higgins and Schubert (1993, 1994) in the summer over Asia and the Pacific, require further study. Since our focus was on the characteristics of the 10–25-day disturbance itself, scale interactions were not considered here. The interannual variability of convection and the activity of transient eddies on this timescale and their relation to ENSO and the tropospheric biennial oscillation is also an interesting topic for future research.

### Acknowledgments

We wish to acknowledge the insightful comments and suggestions from anonymous reviewers and Dr. N. Iwasaka. They were extremely valuable in revising an earlier version of this manuscript. We would also like to thank Dr. R. Kawamura for encouragement and useful discussion. This paper is part of the Ph.D. thesis of Y. Fukutomi of the Institute of Geoscience, University of Tsukuba. ECMWF analyses were kindly provided by Dr. H.L. Tanaka and are the same as those used by Tanaka and Kimura (1997). The OLR data were obtained from the NOAA Climate Diagnostics Center (<http://www.cdc.noaa.gov>). Figures were made with the Generic Mapping Tools (GMT) graphics system developed by Wessel and Smith (1995). This study was supported in part by a Grant-in-Aid for Scientific Research on Priority Areas (B) from the Japanese Ministry of Education, Science, Sports, and Culture, No. 11201101 (Energy and Water Cycle in Asian Monsoon Region), and was completed under the auspices of the Hydrological Cycle Research Program of the FRSGC.

## References

- Ambrizzi, T., B.J. Hoskins, and H.-H. Hsu, 1995: Rossby wave propagation and teleconnection patterns in the austral winter. *J. Atmos. Sci.*, **52**, 3661–3672.
- Cai, M. and M. Mak, 1990: On the basic dynamics of regional cyclogenesis. *J. Atmos. Sci.*, **47**, 1417–1442.
- Chen, T.-C. and J.-M. Chen, 1995: An observational study of the South China Sea monsoon during the 1979 summer: Onset and life cycle. *Mon. Wea. Rev.*, **123**, 2295–2318.
- and S.-P. Weng, 1999: Interannual and intraseasonal variations in monsoon depressions and their westward-propagating predecessors. *Mon. Wea. Rev.*, **127**, 1005–1020.
- Fukutomi, Y. and T. Yasunari, 1999: 10–25-day intraseasonal variations of convection and circulation over East Asia and western North Pacific during early summer. *J. Meteor. Soc. Japan*, **77**, 753–769.
- , 2000: Tropical–extratropical interactions on the intraseasonal timescales over the western Pacific during early summer. Ph.D. thesis, Institute of Geoscience, University of Tsukuba, 162 pp.
- Hartmann, D.L., M.L. Michelsen, and S.A. Klein, 1992: Seasonal variations of tropical intraseasonal oscillations: A 20–25-day oscillation in the western Pacific. *J. Atmos. Sci.*, **49**, 1277–1289.
- Hendon, H.H. and D.L. Hartmann, 1985: Variability in a nonlinear model of the atmosphere with zonally symmetric forcing. *J. Atmos. Sci.*, **42**, 2783–2797.
- Heta, Y., 1990: An analysis of tropical wind fields in relation to typhoon formation over the western Pacific. *J. Meteor. Soc. Japan*, **68**, 65–77.
- Higgins, R.W. and S.D. Schubert, 1993: Low-frequency synoptic-eddy activity in the Pacific storm track. *J. Atmos. Sci.*, **50**, 1672–1690.
- and ———, 1994: Simulated life cycles of persistent anticyclonic anomalies over the North Pacific: role of synoptic-scale eddies. *J. Atmos. Sci.*, **51**, 3238–3260.
- Hoskins, B.J., I.N. James, and G.H. White, 1983: The shape, propagation and mean-flow interaction of large-scale weather systems. *J. Atmos. Sci.*, **40**, 1595–1612.
- and T. Ambrizzi, 1993: Rossby wave propagation on a realistic longitudinally varying flow. *J. Atmos. Sci.*, **50**, 1661–1671.
- Hsu, H.-H., 1996: Global view of the intraseasonal oscillation during northern winter. *J. Climate*, **9**, 2386–2406.
- Hurrell, J.W. and D.G. Vincent, 1991: On the maintenance of short-term subtropical wind maxima in the Southern Hemisphere during SOP-1, FGGE. *J. Climate*, **4**, 1009–1022.
- Jin, F. and B.J. Hoskins, 1995: The direct response to tropical heating in a baroclinic atmosphere. *J. Atmos. Sci.*, **52**, 307–319.
- Karoly, D.J. and B.J. Hoskins, 1982: Three-dimensional propagation of planetary waves. *J. Meteor. Soc. Japan*, **60**, 109–123.
- Kawamura, R. and T. Murakami, 1995: Interaction between the mean summer monsoon flow and 45-day transient perturbations. *J. Meteor. Soc. Japan*, **73**, 1087–1114.
- Kaylor, R.E., 1977: Filtering and decimation of digital time series. Tech. Note BN 850, Institute of Physical Science Technology, University of Maryland, College Park, 42 pp.
- Kiladis, G.N. and K.M. Weickmann, 1992a: Circulation anomalies associated with tropical convection during northern winter. *Mon. Wea. Rev.*, **120**, 1900–1923.
- and ———, 1992b: Extratropical forcing of tropical convection during northern winter. *Mon. Wea. Rev.*, **120**, 1924–1938.
- , G.A. Meehl, and K.M. Weickmann, 1994: Large-scale circulation associated with westerly wind bursts and deep convection over the western equatorial Pacific. *J. Geophys. Res.*, **99**(D9), 18527–18544.
- and M. Wheeler, 1995: Horizontal and vertical structure of observed tropospheric equatorial Rossby waves. *J. Geophys. Res.*, **100**(D11), 22981–22997.
- and K.M. Weickmann, 1997: Horizontal structure and seasonality of large-scale circulations associated with submonthly tropical convection. *Mon. Wea. Rev.*, **125**, 1997–2013.
- , 1998: Observations of Rossby waves linked to convection over the eastern tropical Pacific. *J. Atmos. Sci.*, **55**, 321–339.
- Lau, K.-H. and N.-C. Lau, 1990: Observed structure and propagation characteristics of tropical summertime synoptic scale disturbances. *Mon. Wea. Rev.*, **118**, 1888–1913.
- and ———, 1992: The energetics and propagation dynamics of tropical summertime synoptic-scale disturbances. *Mon. Wea. Rev.*, **120**, 2523–2539.
- Li, L. and T.R. Nathan, 1994: The global atmospheric response to low-frequency tropical forcing: Zonally averaged basic states. *J. Atmos. Sci.*, **51**, 3412–3426.
- and ———, 1997: Effects of low-frequency Tropical Forcing on intraseasonal tropical–extratropical interactions. *J. Atmos. Sci.*, **54**, 332–346.

- Liebmann, B., G.N. Kiladis, J.A. Marengo, T. Ambrizzi, and J.D. Glick, 1999: Submonthly convective variability over South America and the south Atlantic convergence zone. *J. Climate*, **12**, 1877–1891.
- Madden, R.A. and P.R. Julian, 1972: Description of global scale circulation cells in the tropics with a 40–50 day period. *J. Atmos. Sci.*, **29**, 1109–1123.
- and ———, 1994: Observations of the 40–50-day tropical oscillation: A review. *Mon. Wea. Rev.*, **122**, 814–837.
- Magaña, V. and M. Yanai, 1991: Tropical–midlatitude interaction on the time scale of 30 to 60 days during the northern summer of 1979. *J. Climate*, **4**, 180–201.
- Matsumoto, J., 1992: The seasonal changes in Asian and Australian monsoon regions. *J. Meteor. Soc. Japan*, **70**, 257–273.
- Matthews, A.J. and G.N. Kiladis, 1999a: The tropical–extratropical interaction between high-frequency transients and the Madden–Julian oscillation. *Mon. Wea. Rev.*, **127**, 661–677.
- and ———, 1999b: Interactions between ENSO, transient circulation, and tropical convection over the Pacific. *J. Climate*, **12**, 3062–3086.
- Meehl, G.A., G.N. Kiladis, K.M. Weickmann, M. Wheeler, D.S. Gutzler, and G.P. Compo, 1996: Modulation of equatorial subseasonal convective episodes by tropical–extratropical interaction in the Indian and Pacific Ocean regions. *J. Geophys. Res.*, **101**(D10), 15033–15049.
- Mo, K.C., 1999: Alternating wet and dry episodes over California and intraseasonal oscillations. *Mon. Wea. Rev.*, **127**, 2759–2776.
- , 2000: Intraseasonal modulations of summer precipitation over North America. *Mon. Wea. Rev.*, **128**, 1490–1505.
- Murakami, T. and J. Matsumoto, 1994: Summer monsoon over the Asian continent and Western Pacific. *J. Meteor. Soc. Japan*, **72**, 719–745.
- Newman, M. and P.D. Sardeshmukh, 1998: The impact of the annual cycle on the North Pacific/North American response to remote low-frequency forcing. *J. Climate*, **11**, 2491–2504.
- Numaguti, A., 1995: Characteristics of 4-to-20-day-period disturbances observed in the equatorial Pacific during the TOGA COARE IOP. *J. Meteor. Soc. Japan*, **73**, 353–377.
- Plumb, R.A., 1986: Three-dimension propagation of transient quasi-geostrophic eddies and its relationship with the eddy forcing of the time-mean flow. *J. Atmos. Sci.*, **43**, 1657–1678.
- Robinson, W.A., 1993: Mechanisms of low-frequency variability in a simple model with orography. *J. Atmos. Sci.*, **50**, 878–888.
- Salustri, G. and P.H. Stone, 1983: A diagnostic study of the forcing of the Ferrel cell by eddies with latent heat effects included. *J. Atmos. Sci.*, **40**, 1101–1109.
- Schrage, J.M. and D.G. Vincent, 1996: Tropical convection on 7–21 day timescales over the Western Pacific. *J. Climate*, **9**, 587–607.
- Schnadt, C., A. Fink, D.G. Vincent, J.M. Schrage, and P. Speth, 1998: Tropical cyclones, 6–25 day oscillations, and tropical–extratropical interaction over the northwestern Pacific. *Meteor. Atmos. Phys.*, **68**, 151–169.
- Sobel, A.H. and C.S. Bretherton, 1999: Development of synoptic-scale disturbances over the summertime tropical northwest Pacific. *J. Atmos. Sci.*, **56**, 3106–3127.
- Tanaka, H.L. and K. Kimura, 1998: Time series analysis of natural variability in barotropic energy of the atmosphere with ECMWF global analysis. *J. Meteor. Soc. Japan*, **76**, 207–274.
- Trenberth, K.E., 1986: An assessment of the impact of transient eddies on zonal flow during a blocking episode using localized Eliassen–Palm flux diagnostics. *J. Atmos. Sci.*, **43**, 2070–2087.
- , 1991: Storm tracks in the Southern Hemisphere. *J. Atmos. Sci.*, **48**, 2159–2178.
- and J.G. Olson, 1988: An evaluation and intercomparison of global analyses from the National Meteorological Center and the European Center for Medium Range Weather Forecasts. *Bull. Amer. Meteor. Soc.*, **69**, 1047–1057.
- Vincent, D.G., K.-C. Ko, and J.M. Schrage, 1997: Subtropical jet streaks over the South Pacific. *Mon. Wea. Rev.*, **125**, 438–447.
- , A. Fink, J.M. Schrage, and P. Speth, 1998: High- and low-frequency intraseasonal variance of OLR on annual and ENSO timescales. *J. Climate*, **11**, 968–986.
- Webster, P.J. and H.-R. Chang, 1988: Equatorial energy accumulation and emanation regions: Impacts of a zonally varying basic state. *J. Atmos. Sci.*, **45**, 803–829.
- and S. Yang, 1989: The three-dimensional structure of perturbation kinetic energy and its relationship to the zonal wind field. *J. Climate*, **2**, 1210–1222.
- Wheeler, M. and G.N. Kiladis, 1999: Convectively coupled equatorial waves: Analysis of clouds and temperature in the wavenumber-frequency domain. *J. Atmos. Sci.*, **56**, 374–399.
- Wessel, P. and W.H.F. Smith, 1995: New version of the Generic Mapping Tools released. *EOS Trans. Amer. Geophys. U.*, **76**, 329.